Biogeosciences, 17, 741–756, 2020
https://doi.org/10.5194/bg-17-741-2020

Biogeosciences Open Access EGU

Evaluation of bacterial glycerol dialkyl glycerol tetraether and ^{2}H–^{18}O biomarker proxies along a central European topsoil transect

Johannes Hepp[1,2], Imke Kathrin Schäfer[3], Verena Lanny[4], Jörg Franke[3], Marcel Bliedtner[3,a], Kazimierz Rozanski[5], Bruno Glaser[2], Michael Zech[2,6], Timothy Ian Eglinton[4], and Roland Zech[3,a]

[1]Chair of Geomorphology and BayCEER, University of Bayreuth, 95440 Bayreuth, Germany
[2]Institute of Agronomy and Nutritional Sciences, Soil Biogeochemistry, Martin Luther University Halle-Wittenberg, 06120 Halle, Germany
[3]Institute of Geography and Oeschger Centre for Climate Change Research, University of Bern, 3012 Bern, Switzerland
[4]Department of Earth Science, ETH Zurich, 8092 Zurich, Switzerland
[5]Faculty of Physics and Applied Computer Science, AGH University of Science and Technology, 30-059 Cracow, Poland
[6]Institute of Geography, Faculty of Environmental Sciences, Technical University of Dresden, 01062 Dresden, Germany
[a]now at: Institute of Geography, Chair of Physical Geography, Friedrich Schiller University Jena, 07743 Jena, Germany

Correspondence: Johannes Hepp (johannes-hepp@gmx.de)

Received: 20 May 2019 – Discussion started: 29 May 2019
Revised: 4 December 2019 – Accepted: 6 January 2020 – Published: 12 February 2020

Abstract. Molecular fossils, like bacterial branched glycerol dialkyl glycerol tetraethers (brGDGTs), and the stable isotopic composition of biomarkers, such as $\delta^{2}H$ of leaf wax-derived n-alkanes ($\delta^{2}H_{n\text{-alkane}}$) or $\delta^{18}O$ of hemicellulose-derived sugars ($\delta^{18}O_{sugar}$), are increasingly used for the reconstruction of past climate and environmental conditions. Plant-derived $\delta^{2}H_{n\text{-alkane}}$ and $\delta^{18}O_{sugar}$ values record the isotopic composition of plant source water ($\delta^{2}H_{source\text{-}water}$ and $\delta^{18}O_{source\text{-}water}$), which usually reflects mean annual precipitation ($\delta^{2}H_{precipiation}$ and $\delta^{18}O_{precipiation}$), modulated by evapotranspirative leaf water enrichment and biosynthetic fractionation (ε_{bio}). Accuracy and precision of respective proxies should be ideally evaluated at a regional scale. For this study, we analysed topsoils below coniferous and deciduous forests as well as grassland soils along a central European transect in order to investigate the variability and robustness of various proxies and to identify effects related to vegetation. Soil pH values derived from brGDGTs correlate reasonably well with measured soil pH values but are systematically overestimated ($\Delta pH = 0.6 \pm 0.6$). The branched vs. isoprenoid tetraether index (BIT) can give some indication whether the pH reconstruction is reliable. Temperatures derived from brGDGTs overestimate mean annual air temperatures slightly ($\Delta T_{MA} = 0.5\,°C \pm 2.4$). Apparent isotopic fractionation ($\varepsilon_{n\text{-alkane/precipitation}}$ and $\varepsilon_{sugar/precipitation}$) is lower for grassland sites than for forest sites due to signal damping; i.e. grass biomarkers do not record the full evapotranspirative leaf water enrichment. Coupling $\delta^{2}H_{n\text{-alkane}}$ with $\delta^{18}O_{sugar}$ allows us to reconstruct the stable isotopic composition of the source water more accurately than without the coupled approach ($\Delta\delta^{2}H = \sim -21\,‰ \pm 22\,‰$ and $\Delta\delta^{18}O = \sim -2.9\,‰ \pm 2.8\,‰$). Similarly, relative humidity during daytime and the vegetation period (RH_{MDV}) can be reconstructed using the coupled isotope approach ($\Delta RH_{MDV} = \sim -17 \pm 12$). Especially for coniferous sites, reconstructed RH_{MDV} values as well as source water isotope composition underestimate the measured values. This can likely be explained by understorey grass vegetation at the coniferous sites contributing significantly to the n-alkane pool but only marginally to the sugar pool in the topsoils. Vegetation-dependent variable signal damping and ε_{bio} (regarding ^{2}H between n-alkanes and leaf water) along our European transect are difficult to quantify but likely contribute to the observed underestimation in the source water isotope composition and RH reconstructions. Microclimate variability could cause the rather large uncertainties. Vegetation-related effects do, by contrast, not affect the brGDGT-derived reconstructions. Overall, GDGTs and the coupled $\delta^{2}H_{n\text{-alkane}}$–$\delta^{18}O_{sugar}$ approach have great potential for more quantitative paleoclimate reconstructions.

Published by Copernicus Publications on behalf of the European Geosciences Union.

1 Introduction

Information about the variability and consequences of past climate changes is a prerequisite for precise predictions regarding the present climate change. Molecular fossils, so-called biomarkers, have great potential to enhance our understanding about variations in past climate and environmental changes. Lipid biomarkers in particular are increasingly used for paleoclimate and environmental reconstructions (e.g. Brincat et al., 2000; Eglinton and Eglinton, 2008; Rach et al., 2014; Romero-Viana et al., 2012; Schreuder et al., 2016). However strengths and limitations of respective proxies need to be known (Dang et al., 2016). For this, calibrations using modern reference samples are essential.

One famous and widely applied lipid biomarker group are terrestrial branched glycerol dialkyl glycerol tetraethers (brGDGTs). They are synthesised in the cell membranes of anaerobe heterotrophic soil bacteria (Oppermann et al., 2010; Weijers et al., 2010) and have great potential for the reconstruction of past environmental conditions (e.g. Coffinet et al., 2017; Schreuder et al., 2016; R. Zech et al., 2012), although some uncertainties exist. Calibration studies suggest that the relative abundance of the individual brGDGTs varies with mean annual air temperature (T_{MA}) and soil pH (Peterse et al., 2012; Weijers et al., 2007), at least across large, global climate gradients or along pronounced altitudinal gradients (Wang et al., 2017). However, in arid regions the production of brGDGT is limited, while isoprenoidal GDGTs (iGDGTs) produced by archaea provide the dominant part of the overall soil GDGT pool (Anderson et al., 2014; Dang et al., 2016; Dirghangi et al., 2013; Wang et al., 2013; Xie et al., 2012). The ratio of brGDGTs vs. isoprenoid GDGTs (BIT) can be used as an indication of whether a reconstruction of T_{MA} and pH will be reliable. Moreover, Mueller-Niggemann et al. (2016) revealed an influence of the vegetation cover on the brGDGT producing soil microbes. From field experiments, it is known that vegetation type and mulching practice strongly effect soil temperature and moisture (Awe et al., 2015; Liu et al., 2014). Thus, multiple factors can be expected to influence soil microbial communities and GDGT production. So far, little is known about the variability of GDGT proxies on a regional scale, and a calibration study with a small climate gradient but with different vegetation types might be useful.

Concerning paleohydrology proxies, compound-specific stable hydrogen isotopes of leaf wax biomarkers, such as long-chain n-alkanes ($\delta^2H_{n\text{-alkanes}}$), record the isotopic signal of precipitation and therefore past climate and environmental conditions (Sachse et al., 2004, 2006). However, various influencing factors are known, e.g. the moisture source to leaf waxes (Pedentchouk and Zhou, 2018 and Sachse et al., 2012, for review). Next is the evapotranspiration of leaf water (Feakins and Sessions, 2010; Kahmen et al., 2013; Zech et al., 2015), which is strongly driven by relative air humidity (RH; e.g. Cernusak et al., 2016 for review). In addition, a strong precipitation signal is known to be incorporated into long-chain leaf waxes (Hou et al., 2008; Rao et al., 2009; Sachse et al., 2004). In paleoclimate studies, it is often not feasible to disentangle between the evapotranspirative enrichment and the precipitation signal. Zech et al. (2013) proposed coupling $\delta^2H_{n\text{-alkane}}$ results with oxygen stable isotopes of hemicellulose-derived sugars ($\delta^{18}O_{sugar}$). Assuming constant biosynthetic fractionation (ε_{bio}) for the different compound classes (n-alkanes and hemicellulose sugars), this coupling enables the reconstruction of the isotopic composition of leaf water, RH, δ^2H and $\delta^{18}O$ of plant source water ($\approx \delta^2H$ and $\delta^{18}O$ of precipitation; Tuthorn et al., 2015). So far, a detailed evaluation of this approach on the European scale, as well as related effects concerning vegetation changes, is missing.

We analysed topsoil samples under coniferous, deciduous and grassland vegetation along a central European transect in order to estimate the variability of the biomarker proxies. More specifically, we aim to test whether

i. the vegetation type has an influence on the brGDGT proxies, the $\delta^2H_{n\text{-alkane}}$ and the $\delta^{18}O_{sugar}$ stable isotopic composition, and the reconstructed $\delta^2H_{source\text{-}water}$, $\delta^{18}O_{source\text{-}water}$ and RH;

ii. the published brGDGT proxies used for reconstructing mean annual temperature and soil pH are sensitive enough to reflect the medium changes in temperature and soil pH along our transect;

iii. the coupled $\delta^2H_{n\text{-alkane}}$–$\delta^{18}O_{sugar}$ approach enables a δ^2H and $\delta^{18}O$ of precipitation and RH reconstruction along the transect.

2 Material and methods

2.1 Geographical setting and sampling

In November 2012, we collected 29 topsoil samples (0–5 cm depth) from 16 locations along a transect from southern Germany to southern Sweden (Fig. 1a). We distinguished between sites with coniferous forest (con, $n = 9$), deciduous forest (dec, $n = 14$) and grassland (grass, $n = 6$) vegetation cover (for more details see Schäfer et al., 2016, and Table S1 in the Supplement).

2.2 Database of instrumental climate variables and isotope composition of precipitation

Climate data were derived from close-by weather observation stations operated by regional institutions (Deutscher Wetterdienst (DWD) for Germany, Danmarks Meteorologiske Institut (DMI) for Denmark and the Sveriges Meteorologiska och Hydrologiska Institute (SMHI) for Sweden). The DWD provides hourly data for each station (DWD Climate Data Center, 2018b), enabling not only the calculation of T_{MA}, but also of the mean annual relative air humidity

(RH_{MA}), mean temperature and relative air humidity during the vegetation period (T_{MV} and RH_{MV}), and daytime temperature and relative humidity averages over the vegetation period (T_{MDV} and RH_{MDV}). In addition, annual precipitation observations were used to derive the mean annual precipitation amount (P_{MA}; DWD Climate Data Center, 2018a). From the DMI, the respective climate variables were derived from published technical reports (Cappelen, 2002; Frich et al., 1997; Laursen et al., 1999). The SMHI provides open data from which we derived the climate variables for the Swedish sites (Swedish Meteorological and Hydrological Institute, 2018). For more details about the climate database used for calculations and comparisons, the reader is referred to Table S2.

For comprising German precipitation (δ^2H and $\delta^{18}O$) along the transect, we realised a regionalisation (called δ^2H_{GIPR} and $\delta^{18}O_{GIPR}$) using online available data from 34 German GNIP stations, four Austrian ANIP stations and the Groningen GNIP station (van Geldern et al., 2014; IAEA/WMO, 2018; Stumpp et al., 2014; Umweltbundesamt GmbH, 2018), following the approach of Schlotter (2007). However, instead of the multivariate regression procedure applied by Schlotter (2007), we used a random forest approach (Hothorn et al., 2006; Strobl et al., 2007, 2008) to describe the relationship of squared latitude, latitude, longitude and altitude vs. long-term weighted means of precipitation δ^2H and $\delta^{18}O$ and realised the prediction for each site (see the Supplement for more information). For the Danish and Swedish sites, such a procedure was not possible. Hence, the annual precipitation δ^2H and $\delta^{18}O$ values were derived from the Online Isotopes in Precipitation Calculator (OIPC, version 3.1), therefore called δ^2H_{OIPC} and $\delta^{18}O_{OIPC}$ (Bowen, 2018; Bowen and Revenaugh, 2003; IAEA/WMO, 2015). The final used $\delta^2H_{GIPR,OIPC}$ and $\delta^{18}O_{GIPR,OIPC}$ data are given in Table S1.

The T_{MA} along the transect ranges from 5.3 to 10.6 °C, and P_{MA} ranges from 554 to 1769 mm (Fig. 1b). Precipitation δ^2H and $\delta^{18}O$ shows moderate changes along the transect, $\delta^2H_{GIPR,OIPC}$ varies between −52 ‰ and −79 ‰, and $\delta^{18}O_{GIPR,OIPC}$ ranges from −7.4 ‰ to −10.9 ‰ (Fig. 1c).

Correlations between $\delta^{18}O_{GIPR,OIPC}$ and P_{MA}, altitude of the locations, and T_{MA} are given in the Supplement (Figs. S1 to S3), along with a $\delta^2H_{GIPR,OIPC}$ vs. $\delta^{18}O_{GIPR,OIPC}$ scatter plot (Fig. S4).

2.3 Soil extractions and analysis

2.3.1 GDGTs and pH

A detailed description of sample preparation for lipid analysis can be found in Schäfer et al. (2016). Briefly, 1–6 g of freeze-dried and ground soil sample was microwave extracted with 15 mL dichloromethane (DCM) / methanol (MeOH) 9 : 1 ($v : v$) at 100 °C for 1 h. Extracts were separated over aminopropyl silica gel (Supelco, 45 µm) pipette columns. The nonpolar fraction (including n-alkanes) was eluted with hexane and further purified over $AgNO_3$-coated silica pipette columns (Supelco, 60–200 mesh) and zeolite (GHGeochem Ltd.). The GDGT-containing fraction was eluted with DCM : MeOH 1 : 1 ($v : v$), redissolved in hexane / isopropanol 99 : 1 ($v : v$) and transferred over 0.45 µm PTFE filters into 300 µL inserts. For quantification, a known amount of a C46 diol standard was added after transfer. The samples were analysed at ETH Zurich using an Agilent 1260 Infinity series HPLC–atmospheric chemical pressure ionisation mass spectrometer (HPLC-APCI-MS) equipped with a Grace Prevail Cyano column (150 mm × 2.1 mm; 3 µm). The GDGTs were eluted isocratically with 90 % A and 10 % B for 5 min and then with a linear gradient to 18 % B for 34 min at 0.2 mL min^{-1}, where A is hexane and B is hexane / isopropanol (9 : 1, $v : v$). Injection volume was 10 µL and single ion monitoring of $[M+H]^+$ was used to detect GDGTs.

The pH of the samples was measured in the laboratory of the Soil Biogeochemistry group, Institute of Agronomy and Nutritional Sciences, Martin Luther University Halle-Wittenberg, using a pH meter in a 1 : 3 soil : water (w/v) mixture.

2.3.2 δ^2H $_{n\text{-alkane}}$

The hydrogen isotopic composition of the highest concentrated n-alkanes (n-C_{25}, n-C_{27}, n-C_{29}, n-C_{31} and n-C_{33}) was determined using a TRACE GC Ultra gas chromatography connected to a Delta V Plus isotope ratio mass spectrometer via a ^2H pyrolysis reactor kept at 1420 °C (GC-^2H-Py-IRMS; Thermo Scientific, Bremen, Germany) at ETH Zurich (Christoph et al., 2019). For more details about n-alkane quantification the reader is refereed to Schäfer et al. (2016). The compound-specific $^2H/^1H$ ratios were calibrated against an external standard with C_{15}–C_{35} homologues. External standard mixtures (A4 mix from Arndt Schimmelmann, University of Indiana) were run between the samples for multipoint linear normalisation. The H_3^+ factor was determined on each measurement day and was constant throughout the periods of the sample batches. Samples were analysed in duplicates, and results typically agreed within 4 % (average difference = 1.4 %). All δ^2H values are expressed relative to the Vienna Standard Mean Ocean Water (V-SMOW).

2.3.3 $\delta^{18}O_{sugar}$

Hemicellulose sugars were extracted and purified using a slightly modified standard procedure (Amelung et al., 1996; Guggenberger et al., 1994; Zech and Glaser, 2009). Briefly, myo-inositol was added to the samples prior to extraction as the first internal standard. The sugars were released hydrolytically using 4 M trifluoroacetic acid for 4 h at 105 °C, cleaned over glass fibre filters and further purified using XAD and Dowex columns. Before derivatisation with methylboronic

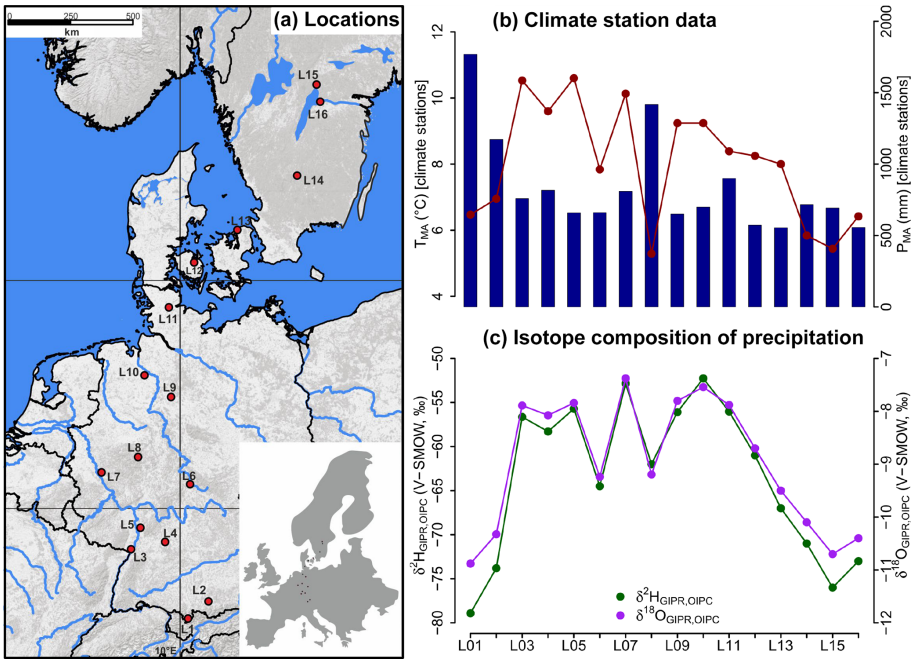

Figure 1. **(a)** Sample locations (red dots, map source: US National Park Service), **(b)** variations of mean annual air temperature (T_{MA}, red dots and line) and mean annual precipitation (P_{MA}, blue bars) derived from close-by climate station data, and **(c)** hydrogen and oxygen stable isotope composition of precipitation ($\delta^{2}H_{GIPR,OIPC}$ and $\delta^{18}O_{GIPR,OIPC}$, respectively) as derived for the sampled transect locations (see Sect. 2.2 GIPR $\delta^{2}H$ and $\delta^{18}O$ generation procedure). The reader is referred to Sect. 2.2 (and Tables S1 and S2) for database and reference information of data plotted in **(b)** and **(c)**.

acid (Knapp, 1979), the samples were frozen and freeze-dried, and 3-O-methylglucose in dry pyridine was added as the second internal standard. Compound-specific hemicellulose sugar ^{18}O measurements were performed in the laboratory of the Soil Biogeochemistry group, Institute of Agronomy and Nutritional Sciences, Martin Luther University Halle-Wittenberg, using GC-^{18}O-Py-IRMS (all devices from Thermo Fisher Scientific, Bremen, Germany). Standard deviations of the triplicate measurements were 1.4 ‰ (over 29 investigated samples) for arabinose and xylose. We focus on these two hemicellulose-derived neutral sugars arabinose and xylose as they strongly predominate over fucose in terrestrial plants, soils and sediments (Hepp et al., 2016, and references therein). Rhamnose concentrations were too low to obtain reliable $\delta^{18}O$ results. All $\delta^{18}O$ values are expressed relative to the Vienna Standard Mean Ocean Water (V-SMOW).

2.4 Theory and calculations

2.4.1 Calculations used for the GDGT-based reconstructions

The branched and isoprenoid tetraether (BIT) index is calculated according to Hopmans et al. (2004); for structures see Fig. S5:

$$\mathrm{BIT} = \frac{\mathrm{Ia} + \mathrm{IIa} + \mathrm{IIIa}}{\mathrm{Ia} + \mathrm{IIa} + \mathrm{IIIa} + \mathrm{crenarchaeol}}. \quad (1)$$

The cyclopentane moiety number of brGDGTs correlates negatively with soil pH (Weijers et al., 2007), which led to the development of the ratio of cyclisation of branched tetraethers (CBT). CBT and the CBT-based pH ($\mathrm{pH_{CBT}}$) were calculated according to Peterse et al. (2012):

$$\mathrm{CBT} = \log \frac{\mathrm{Ib} + \mathrm{IIb}}{\mathrm{Ia} + \mathrm{IIa}}, \quad (2)$$

$$\mathrm{pH_{CBT}} = 7.9 - 1.97 \times \mathrm{CBT}. \quad (3)$$

The number of methyl groups in brGDGTs correlates negatively with T_{MA} and soil pH (Peterse et al., 2012; Weijers et al., 2007). Thus, the ratio of the methylation of branched tetraethers (MBT) and the CBT ratio can be used to reconstruct T_{MA}. We use the equation given by Peterse et al. (2012):

$$\mathrm{MBT'} = \frac{\mathrm{Ia} + \mathrm{Ib} + \mathrm{Ic}}{\mathrm{Ia} + \mathrm{Ib} + \mathrm{Ic} + \mathrm{IIa} + \mathrm{IIb} + \mathrm{IIc} + \mathrm{IIIa}}, \quad (4)$$

$$T_{MA} = 0.81 - 5.67 \times \mathrm{CBT} + 31.0 \times \mathrm{MBT'}. \quad (5)$$

2.4.2 Calculations and concepts used for the coupled δ^2H–δ^{18}O approach

The apparent fractionation is calculated according to Cernusak et al. (2016):

$$\varepsilon_{n\text{-alkane/precipitation}} = \left(\frac{\delta^2 H_{n\text{-alkane}} - \delta^2 H_{GIPR,OIPC}}{1 + \delta^2 H_{GIPR,OIPC}/1000} \right), \quad (6)$$

$$\varepsilon_{\text{sugar/precipitation}} = \left(\frac{\delta^{18} O_{\text{sugar}} - \delta^{18} O_{GIPR,OIPC}}{1 + \delta^{18} O_{GIPR,OIPC}/1000} \right). \quad (7)$$

The isotopic composition of leaf water ($\delta^2 H_{\text{leaf-water}}$ and $\delta^{18} O_{\text{leaf-water}}$) can be calculated using ε_{bio} for $\delta^2 H_{n\text{-alkane}}$ (−160 ‰; Sachse et al., 2012; Sessions et al., 1999) and $\delta^{18} O_{\text{sugar}}$ (+27 ‰; Cernusak et al., 2003; Schmidt et al., 2001):

$$\delta^2 H_{\text{leaf-water}} = \left(\frac{1000 + \delta^2 H_{n\text{-alkane}}}{1000 + \varepsilon_{\text{bio}}(n\text{-alkane})} \right) \times 10^3 - 1000, \quad (8)$$

$$\delta^{18} O_{\text{leaf-water}} = \left(\frac{1000 + \delta^{18} O_{\text{sugar}}}{1000 + \varepsilon_{\text{bio}}(\text{sugar})} \right) \times 10^3 - 1000. \quad (9)$$

Zech et al. (2013) introduced the conceptual model for the coupled $\delta^2 H_{n\text{-alkane}}$–$\delta^{18} O_{\text{sugar}}$ approach in detail. Briefly, the coupled approach is based on the following assumptions (illustrated in Fig. 8). (i) The isotopic composition of precipitation, which is set to be equal to the plant source water, typically plots along the global meteoric water line (GMWL; $\delta^2 H = 8 \times \delta^{18} O + 10$) in a $\delta^{18} O$ vs. $\delta^2 H$ space (Craig, 1961). (ii) Source water uptake by plants does not lead to any fractionation (e.g. Dawson et al., 2002), and significant evaporation of soil water can be excluded. (iii) Evapotranspiration leads to enrichment of the remaining leaf water along the local evaporation line (LEL; Allison et al., 1985; Bariac et al., 1994; Walker and Brunel, 1990), compared to the source water taken up by the plant. (iv) The biosynthetic fractionation is assumed to be constant. In addition, isotopic equilibrium between plant source water (∼ weighted mean annual precipitation) and the local atmospheric water vapour is assumed. Further assumption concerns the isotope steady state in the evaporating leaf water reservoir. The coupled approach allows for reconstruction of the isotopic composition of plant source water ($\delta^2 H_{\text{source-water}}$ and $\delta^{18} O_{\text{source-water}}$) from the reconstructed leaf water, by calculating the intercepts of the LELs with the GMWL (Zech et al., 2013). The slope of the LEL (S_{LEL}) can be assessed by the following equation (Gat, 1971):

$$S_{\text{LEL}} = \frac{\varepsilon_2^* + C_k^2}{\varepsilon_{18}^* + C_k^{18}}, \quad (10)$$

where ε^* represents equilibrium isotope fractionation factors and C_k represents kinetic fractionation factors. The latter equals 25.1 ‰ and 28.5 ‰ for C_k^2 and C_k^{18}, respectively (Merlivat, 1978). The equilibrium fractionation factors can be derived from empirical equations (Horita and Wesolowski, 1994) by using T_{MDV} values. For two Danish sites T_{MDV} values are not available; instead T_{MV} is used here (Sect. 2.2 and Table S2).

In a $\delta^{18} O$–$\delta^2 H$ diagram, the distance of the leaf water from the GMWL defines the deuterium excess of leaf water ($d_{\text{leaf-water}} = \delta^2 H_{\text{leaf-water}} - 8 \times \delta^{18} O_{\text{leaf-water}}$, according Dansgaard (1964); Fig. 8). To convert $d_{\text{leaf-water}}$ into mean RH during daytime and the vegetation period (RH_{MDV}), a simplified Craig–Gordon model can be applied (Zech et al., 2013):

$$RH = 1 - \frac{\Delta d}{\varepsilon_2^* - 8 \times \varepsilon_{18}^* + C_k^2 - 8 \times C_k^{18}}, \quad (11)$$

where Δd is the difference in $d_{\text{leaf-water}}$ and the deuterium excess of source water ($d_{\text{source-water}}$).

2.5 Statistics

In the statistical analysis we checked sample distributions for normality (Shapiro and Wilk, 1965) and for equal variance (Levene, 1960). If normality and equal variances are given, we perform an analysis of variance (ANOVA). If that is not the case, we conduct the non-parametric Kruskal–Wallis test. ANOVA or Kruskal–Wallis are used to find significant differences ($a = 0.05$) between the vegetation types (deciduous, conifer and grass).

In order to describe the relation along a 1 : 1 line, the coefficient of correlation (R^2) was calculated as $R^2 = 1 - \sum(\text{modeled} - \text{measured})^2 / \sum(\text{measured} - \text{measured mean})^2$. The small r^2 is taken as coefficient of correlation of a linear regression between a dependent (y) and explanatory variable(s). The root-mean-square error (RMSE) of the relationships was calculated as $\text{RMSE} = \sqrt{\left(\frac{1}{n} \cdot \sum(\text{modeled} - \text{measured})^2\right)}$. All data plotting and statistical analysis was realised in R (version 3.2.2; R Core Team, 2015).

3 Results and discussion

3.1 GDGT concentrations

GDGT Ia has the highest concentration under all vegetation types, followed by GDGT IIa and GDGT IIIa (Fig. 2). GDGT Ib, IIb and Ic occur in minor amounts and GDGT IIc and IIIb only in trace amounts. GDGT IIIc was below the detection limit in most of the samples (Table S3). Although other studies document an influence of the vegetation cover on soil temperature and soil water content, which control the microbial community composition in soils (Awe et al., 2015; Liu et al., 2014; Mueller-Niggemann et al., 2016), we find no statistically different pattern of the individual brGDGTs.

Total concentrations of brGDGTs range from 0.32 to 9.17 µg g^{-1} dry weight and tend to be highest for the coniferous samples and lowest for the grasses (Fig. 3a, Table S3).

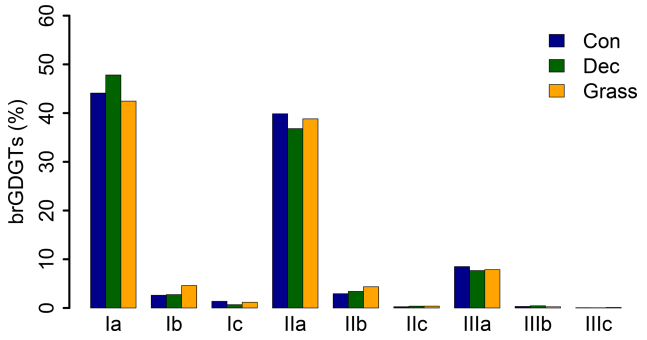

Figure 2. Mean concentrations of individual brGDGTs as percentage of all brGDGTs for the three investigated types. Abbreviations: con: coniferous forest sites ($n = 9$); dec: deciduous forest sites ($n = 14$); grass: grassland sites ($n = 6$).

Bulk brGDGT concentrations lie within the range of other studies examining soils of mid-latitude regions (Huguet et al., 2010a, b; Weijers et al., 2011). Similar concentrations in coniferous and deciduous samples imply that brGDGT production does not strongly vary in soils below different forest types. The grass samples show lower brGDGT concentrations compared to the forest samples, but this is probably mainly due to ploughing of the grass sites in former times and hence admixing of mineral subsoil material. The differences in brGDGT concentrations are not significant (p value $= 0.06$).

3.2 BIT index

Most of the samples have a BIT index higher than 0.9 (Fig. 3b and Table S3). The BIT values are typical for soils in humid and temperate climate regions (Weijers et al., 2006). However, outliers exist. The most likely source of iGDGTs in soils are Thaumarchaeota, i.e. aerobe ammonia oxidising archaea producing Crenarchaeol and its regioisomer (Schouten et al., 2013 and references therein), when the precipitation amount drops below 700–800 mm (Dang et al., 2016; Dirghangi et al., 2013). The P_{MA} data of our sampling sites mostly show precipitation > 550 mm (Fig. 1b), but one has to be aware that these data are based on the climate station closest to the respective sampling locations and that microclimate effects, such as sunlight exposure, canopy cover or exposition, might have a pronounced influence on the brGDGT vs. iGDGT distribution. Mueller-Niggemann et al. (2016) found higher BIT indices in upland soils compared to paddy soils and stated that the management type also influences BIT values in soils. Along our transect, grass sites tend to have slightly lower BIT values than forest sites, probably due to the absence of a litter layer and hence no isolation mechanism preventing evaporation of soil water. Differences between vegetation types are not significant (p value $= 0.32$).

3.3 CBT-derived pH

The CBT ratio shows a pronounced variation independent of vegetation type with values between 0.03 and 2.16 (Fig. 3c). The coniferous samples tend to be highest, but the differences between vegetation types are not significant (p value $= 0.48$). The CBT index can be related to pH in acidic and/or humid soils (e.g. Dirghangi et al., 2013; Mueller-Niggemann et al., 2016; Peterse et al., 2012; Weijers et al., 2007) but might be an indicator of soil water content and hence precipitation in more arid and alkaline soils (e.g. Dang et al., 2016). There is a pronounced correlation between CBT and soil pH (Fig. 4), which is in good agreement with other studies from mid-latitude regions where precipitation is relatively high (Anderson et al., 2014, and references therein). Moreover, the CBT-to-pH relationship in terms of slope and intersect in our dataset ($\mathrm{CBT} = -0.47 \times \mathrm{pH} + 3.5$, $r^2 = 0.7$, p value < 0.0001, $n = 29$) is comparable to the correlation described for the global calibration dataset of Peterse et al. (2012) ($\mathrm{CBT} = -0.36 \times \mathrm{pH} + 3.1$, $r^2 = 0.7$, p value < 0.0001, $n = 176$).

However, there are some outliers in the CBT–pH correlation, which need further examination (see locations grass L04, dec L10 and dec L12 as marked in Figs. 4 and 5). The outliers show lower BIT indices (< 0.85, Table S3). Even though the data from the nearest climate station suggest no abnormal P_{MA}. Local effects such as differences in the amount of sunlight exposure, nutrient availability for brGDGT-producing organisms or most likely soil water content might influence the brGDGT production at these locations (Anderson et al., 2014; Dang et al., 2016). A lower BIT index as well as a lower CBT occur when soil water content decreases (Dang et al., 2016; Sun et al., 2016) or when aeration is high and less anoxic microhabitats for GDGT-producing microbes exist (e.g. Dirghangi et al., 2013).

As the CBT and pH are similarly correlated in our dataset and the global dataset of Peterse et al. (2012), the CBT-derived pH correlated well with the actual pH (Fig. 5a; $R^2 = 0.3$). Expressed as ΔpH (CBT-derived pH – measured pH), there is a tendency that the GDGTs result in an overestimation of the real pH for the forest sites (Fig. 5b). However, a Kruskal–Wallis test shows no statistically significant difference between the vegetation types, with a p value of 0.13. The overall ΔpH of 0.6 ± 0.6 shows that the reconstruction of soil pH using brGDGTs works well along this transect.

3.4 MBT′–CBT-derived T_{MA} reconstructions

The MBT′ shows high variability with values ranging from 0.17 to 0.67 and no statistical differences between vegetation types (p value $= 0.54$; Fig. 3d, Table S3). When comparing reconstructed (MBT′–CBT-derived) T_{MA} with climate station T_{MA}, the data plot close to the 1 : 1 line and fit well into the global dataset of Peterse et al. (2012) (Fig. 6a). The ΔT_{MA} values reveal an overall offset of $0.5\,^{\circ}\mathrm{C} \pm 2.4$, and

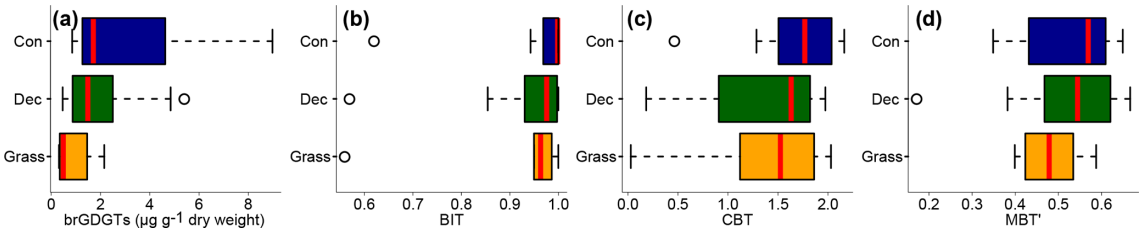

Figure 3. **(a)** Total concentrations of brGDGTs in microgrammes per gramme of dry weight, as well as **(b)** BIT, **(c)** CBT and **(d)** MBT′. Abbreviations: con: coniferous forest sites ($n = 9$); dec: deciduous forest sites ($n = 14$); grass: grassland sites ($n = 6$). Box plots show the median (red line), interquartile range (IQR) with the upper (75 %) and lower (25 %) quartiles, lowest whisker still within 1.5 IQR of the lower quartile, and highest whisker still within 1.5 IQR of the upper quartile; dots mark outliers.

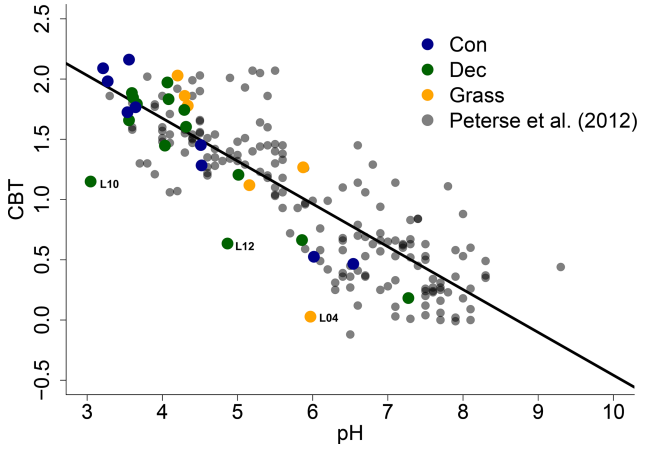

Figure 4. CBT-to-pH relationship in our dataset in comparison to the global calibration dataset from Peterse et al. (2012) ($\mathrm{CBT} = -0.36 \times \mathrm{pH} + 3.1$, $r^2 = 0.7$, p value < 0.0001, $n = 176$, black line). Abbreviations: con: coniferous forest sites ($n = 9$); dec: deciduous forest sites ($n = 14$); grass: grassland sites ($n = 6$).

there is no statistical difference between vegetation types (Fig. 6b). The standard deviation in ΔT_{MA} of ± 2.4 is well in line with the RMSE of 5.0 for the global calibration dataset (Peterse et al., 2012).

3.5 Potential impact of the used liquid chromatography method on pH and T_{MA} reconstructions

The GDGT data presented in this study are not acquired with the up-to-date method (e.g. compare De Jonge et al., 2014 vs. R. Zech et al., 2012). De Jonge et al. (2014) presented a new liquid chromatography method which enables the separation for the brGDGTs with m/z 1036, 1034, 1032, 1050, 1048 and 1046 into 6-methyl and 5-methyl stereoisomers. The old method did not allow such a separation (R. Zech et al., 2012); thus, in the calibration, often the sum of 6 and 5-methylated brGDGTs was used (see and compare De Jonge et al., 2014, vs. Peterse et al., 2012). This introduces scatter to the MBT′–CBT-based T_{MA} reconstructions and can cause a correlation between pH and MBT′ (for more details see De Jonge et al., 2014). De Jonge et al. (2014) moreover show that the 6-methyl brGDGTs are ubiquitously abundant in soils from all over the world, based on reanalysing the dataset of Peterse et al. (2012). However, they also compare reconstructed T_{MA} values based on MBT′–CBT calibration (Peterse et al., 2012) and their newly developed T_{MA} calibration and state that they plot around a 1 : 1 line. They furthermore state that, especially for arid areas, larger deviations can be expected. Finally, they conclude that the use of the newly developed calibrations will improve the T_{MA} and pH reconstructions for areas with arid climate conditions. Because our study transect spans from southern Germany to southern Sweden, representing temperate and humid climate conditions, we argue that the usage of the older liquid chromatography method does not introduce a systematic error in our T_{MA} and pH reconstructions. Still, a higher variability/scatter could be associated with the calibration of Peterse et al. (2012) and therefore also present in our T_{MA} and pH reconstructions.

3.6 Apparent fractionation of $\delta^{2}H$ and $\delta^{18}O$ in the different vegetation types

$\delta^{2}H$ values could be obtained for the n-alkanes C_{27}, C_{29} and C_{31} in all samples and additionally at two locations for n-C_{25} and at six other locations for n-C_{33}. The $\delta^{2}H_{n\text{-alkane}}$ values, calculated as the mean of n-C_{25} to n-C_{31} $\delta^{2}H$, range from -156 ‰ to -216 ‰. Pooled standard deviations show an overall average of 3.6 ‰. The $\delta^{18}O_{\mathrm{sugar}}$ values, calculated as the area-weighted means for arabinose and xylose, range from $+27.7$ ‰ to $+39.4$ ‰. The average weighted mean standard deviation is 1.4 ‰. The compound-specific isotope data are summarised along with the calculations in Table S4.

Apparent fractionation ($\varepsilon_{n\text{-alkane/precipitation}}$) is on the order of -120 ‰ to -150 ‰, i.e. a bit less than the biosynthetic fraction of -160 ‰. This implies that evapotranspirative enrichment is ~ 10 ‰ to 40 ‰ (Fig. 7a). $\varepsilon_{n\text{-alkane/precipitation}}$ is lower for grass sites compared to the forest sites. Differences are significant between deciduous and grass sites (p value $= 0.005$). This finding supports the results of other studies (Kahmen et al., 2013; Liu and Yang, 2008; McInerney et al., 2011) and can be named signal damping. Grasses

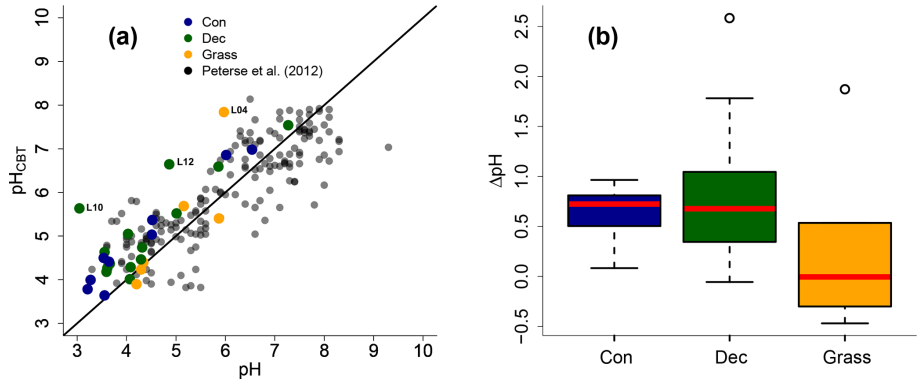

Figure 5. (a) Correlation between measured pH and reconstructed soil pH (pH_{CBT}) from our transect data in comparison to the global calibration dataset from Peterse et al. (2012) ($R^2 = 0.7$, RMSE = 0.75, $n = 176$). The black line indicates the 1 : 1 relationship. **(b)** Box plots of ΔpH (refers to pH_{CBT}–pH). Box plots show the median (red line), interquartile range (IQR) with the upper (75 %) and lower (25 %) quartiles, lowest whisker still within 1.5 IQR of the lower quartile, and highest whisker still within 1.5 IQR of the upper quartile; dots mark outliers. Abbreviations: con: coniferous forest sites ($n = 9$); dec: deciduous forest sites ($n = 14$); grass: grassland sites ($n = 6$).

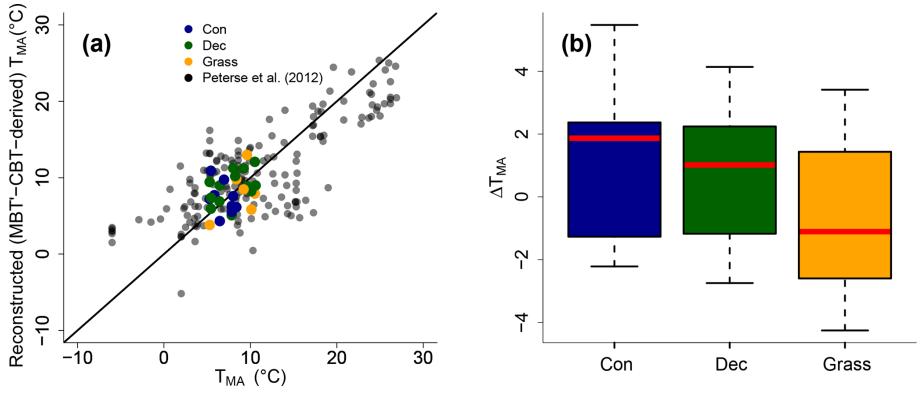

Figure 6. (a) Correlation between climate station T_{MA} and reconstructed (MBT′–CBT-derived) T_{MA}. For comparison, the global calibration dataset from Peterse et al. (2012) is shown. The black line indicates the 1 : 1 relationship. **(b)** Box plots of ΔT_{MA} (refers to reconstructed $T_{MA} - T_{MA}$ from climate stations) in the different vegetation types from our transect study. Box plots show the median (red line), interquartile range (IQR) with the upper (75 %) and lower (25 %) quartiles, lowest whisker still within 1.5 IQR of the lower quartile, and highest whisker still within 1.5 IQR of the upper quartile; dots mark outliers. Abbreviations: con: coniferous forest sites ($n = 9$); dec: deciduous forest sites ($n = 14$); grass: grassland sites ($n = 6$).

do not only incorporate the evaporatively enriched leaf water but also unenriched xylem water in the growth and differentiation zone of grasses (Gamarra et al., 2016; Liu et al., 2017).

The grass-derived hemicellulose sugar biomarkers do not fully record the evapotranspirative enrichment of the leaf water, either, as indicated by lower apparent fractionation ($\varepsilon_{sugar/precipitation}$) in Fig. 7b. The differences are significant between forest and grass sites (p value < 0.005). This is in agreement with a study on cellulose extracted from grass blades (Helliker and Ehleringer, 2002), and again the signal damping can be explained with incorporation of enriched leaf water and non-enriched stem water.

Based on the comparison of evapotranspirative enrichment between forest and grass sites, the signal damping can be quantified to be ∼ 31 % for the hemicellulose sugars and ∼ 49 % for the n-alkanes. This is in agreement with other studies that reported a loss of 22 % of the leaf water enrichment for hemicellulose sugars (Helliker and Ehleringer, 2002) and 39 % to 62 % loss of the leaf water enrichment for n-alkanes (Gamarra et al., 2016).

3.7 $\delta^{2}H_{source\text{-}water}$ and $\delta^{18}O_{source\text{-}water}$ reconstructions

The $\delta^{2}H$ versus $\delta^{18}O$ diagram shown in Fig. 8 graphically illustrates the reconstruction of $\delta^{2}H_{leaf\text{-}water}$ and $\delta^{18}O_{leaf\text{-}water}$ (coloured dots) from $\delta^{2}H_{n\text{-}alkane}$ and $\delta^{18}O_{sugar}$ (crosses), as well as the reconstruction of $\delta^{2}H_{source\text{-}water}$ and $\delta^{18}O_{source\text{-}water}$ (black dots). For reconstructing $\delta^{2}H_{source\text{-}water}$ and $\delta^{18}O_{source\text{-}water}$, LELs with an average slope of 2.8 ± 0.1 (Eq. 10) can be generated through every leaf water point and the intercepts of these LELs with the GMWL.

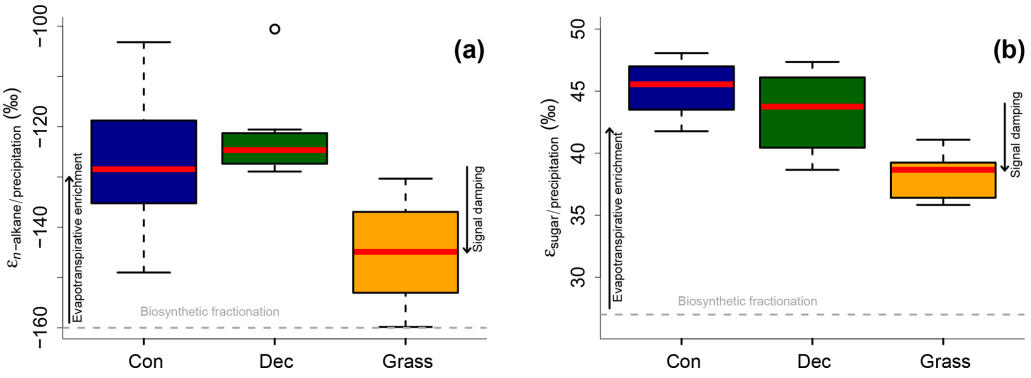

Figure 7. Apparent fractionation **(a)** $\varepsilon_{n\text{-alkane/precipitation}}$ and **(b)** $\varepsilon_{\text{sugar/precipitation}}$. Biosynthetic fractionation factors according to Sect. 2.4.2. Box plots show the median (red line), interquartile range (IQR) with the upper (75 %) and lower (25 %) quartiles, lowest whisker still within 1.5 IQR of the lower quartile, and highest whisker still within 1.5 IQR of the upper quartile; dots mark outliers. Abbreviations: con: coniferous forest sites ($n = 9$); dec: deciduous forest sites ($n = 11$ and 14 for n-alkanes and sugars, respectively); grass: grassland sites ($n = 4$ and 6 for n-alkanes and sugars, respectively). The figure conceptually illustrates the effect of biosynthetic fractionation and evapotranspirative enrichment as well as signal damping.

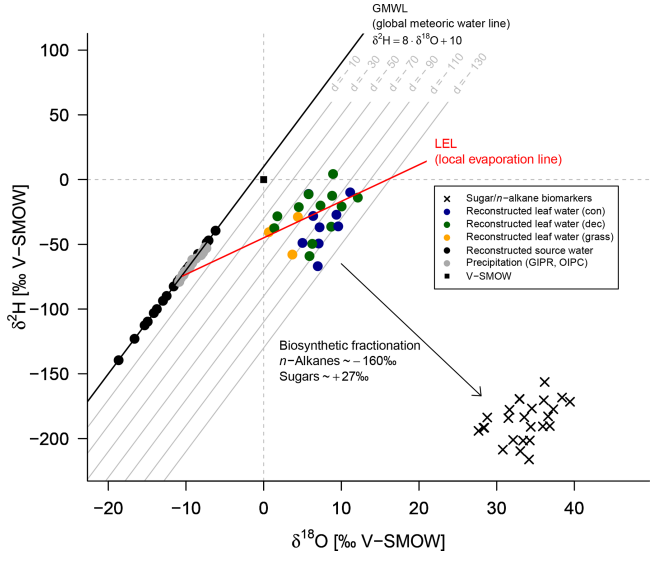

Figure 8. $\delta^{2}H$ vs. $\delta^{18}O$ diagram illustrating the coupled $\delta^{2}H_{n\text{-alkane}}$–$\delta^{18}O_{\text{sugar}}$ approach: measured $\delta^{2}H_{n\text{-alkane}}$ and $\delta^{18}O_{\text{sugar}}$ values, reconstructed $\delta^{2}H_{\text{leaf-water}}$ and $\delta^{18}O_{\text{leaf-water}}$ (according Eqs. 8 and 9), and reconstructed $\delta^{2}H_{\text{source-water}}$ and $\delta^{18}O_{\text{source-water}}$ in comparison to GIPR and OIPC-based $\delta^{2}H_{\text{precipitation}}$ and $\delta^{18}O_{\text{precipitation}}$. Abbreviations: con: coniferous forest sites ($n = 9$); dec: deciduous forest sites ($n = 11$); grass: grassland sites ($n = 4$).

The reconstructed $\delta^{2}H_{\text{source-water}}$ and $\delta^{18}O_{\text{source-water}}$ results can be compared with the $\delta^{2}H_{\text{GIPR,OIPC}}$ and $\delta^{18}O_{\text{GIPR,OIPC}}$ data (Fig. 9). This comparison reveals that the coupled $\delta^{2}H_{n\text{-alkane}}$–$\delta^{18}O_{\text{sugar}}$ approach yields more accurate $\delta^{2}H_{\text{source-water}}$ and $\delta^{18}O_{\text{source-water}}$ compared to single $\delta^{2}H_{n\text{-alkane}}$ approaches. However, the range of the reconstructed $\delta^{2}H_{\text{source-water}}$ and $\delta^{18}O_{\text{source-water}}$ values is clearly larger than in $\delta^{2}H_{\text{GIPR,OIPC}}$ and $\delta^{18}O_{\text{GIPR,OIPC}}$ values. $\delta^{2}H$ is systematically underestimated by $\sim 21\,‰ \pm 22\,‰$ (Fig. 9b) and $\delta^{18}O$ by $\sim 2.9\,‰ \pm 2.8\,‰$ (Fig. 9d). The type of vegetation seems to be not particularly relevant (p value $= 0.18$ for $\Delta\delta^{2}H$ and p value $= 0.34$ for $\Delta\delta^{18}O$). Nevertheless, the systematic offsets tend to be lowest for the deciduous sites ($\Delta\delta^{2}H$ and $\Delta\delta^{18}O$ are closer to zero with $\sim -5\,‰ \pm 15\,‰$ and $\sim -1.1\,‰ \pm 2.1\,‰$), followed by grass sites ($\sim -14\,‰ \pm 20\,‰$ and $\sim -2.1\,‰ \pm 2.6\,‰$). In comparison, the coniferous sites show the largest offsets ($\sim -23\,‰ \pm 26\,‰$ for $\Delta\delta^{2}H$ and $\sim -3.0\,‰ \pm 3.3\,‰$ for $\Delta\delta^{18}O$). Differences are, however, not statistically significant. The systematic offset and the large variability might have more specific reasons, and we suggest that this is related to the type of vegetation. Deciduous trees produce lots of leaf waxes and sugars (e.g. Prietzel et al., 2013; M. Zech et al., 2012a), and all biomarkers reflect and record the evapotranspirative enrichment of the leaf water (e.g. Kahmen et al., 2013; Tuthorn et al., 2014). By contrast, coniferous trees produce quite low amounts of n-alkanes (Diefendorf and Freimuth, 2016; M. Zech et al., 2012a), while sugar concentrations are as high as in other vascular plants (e.g. Hepp et al., 2016; Prietzel et al., 2013). For the coniferous soil samples this means that the n-alkanes stem most likely from the understorey whereas the sugars originate from grasses and coniferous needles. When the understorey is dominated by grass species, the n-alkane biomarkers do not record the full leaf water enrichment signal, whereas the sugars from the needles do. The reconstructed leaf water for the coniferous sites is therefore too negative concerning $\delta^{2}H$, and reconstructed $\delta^{2}H_{\text{source-water}}$ and $\delta^{18}O_{\text{source-water}}$ values thus also become too negative (Fig. 8). Concerning the grass sites, the following explanation can be found. Correcting for signal damping makes the reconstructed leaf water points more positive and shifts them in Fig. 8 up and to the right. As the

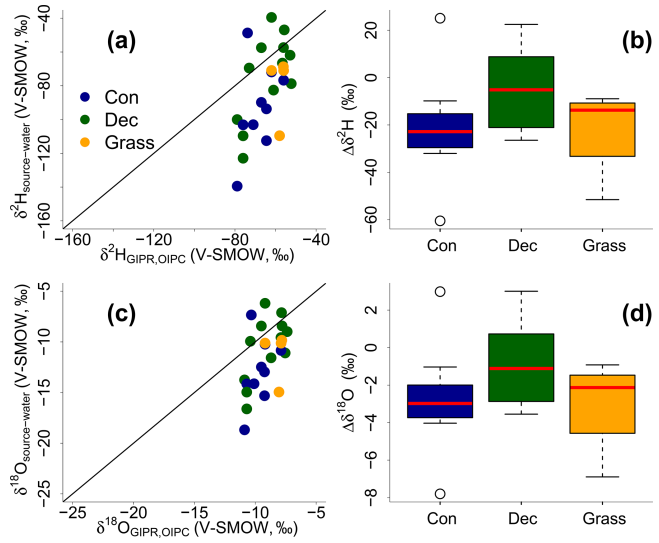

Figure 9. Correlation of reconstructed $\delta^2H_{source\text{-}water}$ and $\delta^{18}O_{source\text{-}water}$ vs. precipitation $\delta^2H_{GIPR,OIPC}$ and $\delta^{18}O_{GIPR,OIPC}$ **(a, c)**. Black lines indicate the 1 : 1 relationship. Differences between reconstructed source water and precipitation ($\Delta\delta^2H = \delta^2H_{source\text{-}water} - \delta^2H_{GIPR,OIPC}$, $\Delta\delta^{18}O = \delta^{18}O_{source\text{-}water} - \delta^{18}O_{GIPR,OIPC}$) for the three different vegetation types **(b, d)**. Box plots show the median (red line), interquartile range (IQR) with upper (75 %) and lower (25 %) quartiles, lowest whisker still within 1.5 IQR of the lower quartile, and highest whisker still within 1.5 IQR of the upper quartile. Abbreviations: con: coniferous forest sites ($n = 9$); dec: deciduous forest sites ($n = 11$); grass: grassland sites ($n = 4$).

signal damping is stronger for δ^2H than for $\delta^{18}O$, the corrected leaf water points would now plot above the uncorrected ones. The corrected leaf water points lead to more positive reconstructed $\delta^2H_{source\text{-}water}$ and $\delta^{18}O_{source\text{-}water}$ values for the grass sites. However, Gao et al. (2014) and Liu et al. (2016) showed that the ε_{bio} (regarding ^2H between n-alkanes and leaf water) of monocotyledon plants could be larger than those of dicotyledonous ones. This would therefore also cause a more negative $\varepsilon_{n\text{-alkane/precipitation}}$ for grasses compared to trees. We observe that the $\varepsilon_{n\text{-alkane/precipitation}}$ is indeed more negative for the grass sites compared to the forest sites (Fig. 7 and Sect. 3.6). Therefore, effects of signal damping vs. variable ε_{bio} along with vegetation types are indistinguishable here. As an outlook for a future study, we therefore strongly recommend a comparison between the here measured $\delta^2H_{n\text{-alkane}}$ values with modelled ones using, for example, the new available model approach from Konecky et al. (2019), which could provide insights if such vegetation effects on ε_{bio} of ^2H in n-alkanes are describable.

Rooting depths specific to vegetation type could partly cause the overall high variability in reconstructed $\delta^2H_{source\text{-}water}$ and $\delta^{18}O_{source\text{-}water}$. Deep-rooting species most likely use the water from deeper soil horizons and/or shallow groundwater, which is equal to the (weighted) mean annual precipitation (e.g. Herrmann et al., 1987). Shallow-rooting plants take up water from upper soil horizons, which is influenced by seasonal variations in $\delta^2H_{precipiation}$ and $\delta^{18}O_{precipiation}$ and by soil water enrichment (Dubbert et al., 2013). Thus, the overall assumption that the source water of the plants reflects the local (weighted) mean precipitation might be not fully valid for all sites. Moreover, a partial contribution of root-derived rather than leaf-derived sugar biomarkers in our topsoil samples is very likely. This does, by contrast, not apply for n-alkanes, which are hardly produced in roots (M. Zech et al., 2012b, and the discussion therein).

Moreover, the high variability within the vegetation types could be caused by variability in ε_{bio} of ^2H in n-alkanes, as well as ^{18}O in sugars. There is an ongoing discussion about the correct ε_{bio} for ^{18}O in hemicellulose sugars (Sternberg, 2014 vs. Zech et al., 2014), and ε_{bio} is probably not constant over all vegetation types. This translates into errors concerning leaf water reconstruction and thus reconstructing $\delta^2H_{source\text{-}water}$ and $\delta^{18}O_{source\text{-}water}$ values (Eq. 9 and Fig. 8). Likewise, the ε_{bio} values reported in the literature for ^2H of n-alkanes can be off from −160 ‰ by tens of per mille (Feakins and Sessions, 2010; Tipple et al., 2015; Feakins et al., 2016; Freimuth et al., 2017). The degree to which hydrogen originates from NADPH rather than leaf water is important, because NADPH is more negative (Schmidt et al., 2003). The wide range in biosynthetic ^2H fractionation factors, which can be even larger, is therefore also related to the carbon and energy metabolism state of plants (Cormier et al., 2018).

3.8 RH reconstruction

Reconstructed RH_{MDV} ranges from 34 % to 74 %, while RH_{MDV} values from climate station data range from 61 % to 78 % (Fig. 10a). Biomarker-based values thus systematically underestimate the station data ($\Delta RH_{MDV} = -17\,\% \pm 12\,\%$). However, the offsets are much less for deciduous tree and grass sites ($\Delta RH_{MDV} = -10\,\% \pm 12\,\%$ and $-7\,\% \pm 9\,\%$, respectively; Fig. 10b). The offsets for the coniferous sites are $-30\,\% \pm 11\,\%$ and significantly larger than for the deciduous and grass sites (p values < 0.05).

Too low reconstructed RH_{MDV} values for the coniferous sites make sense in view of the previously discussed option that soils contain n-alkanes from the understorey (which is dominated by grass species), while sugars stem from needles and grasses. As explained earlier already, the signal damping leads to too negative reconstructed $\delta^2H_{leaf\text{-}water}$ (whereas $\delta^{18}O$ is affected less by the signal damping), and too negative $\delta^2H_{leaf\text{-}water}$ translates into overestimated d-excess and underestimated RH values. In Fig. 8, a correction for this requires moving the coniferous leaf water data points upwards towards more positive δ^2H values; thus the distance between the leaf water and the source water is reduced. It should be noted that here variable ε_{bio} (regarding ^2H between n-alkanes

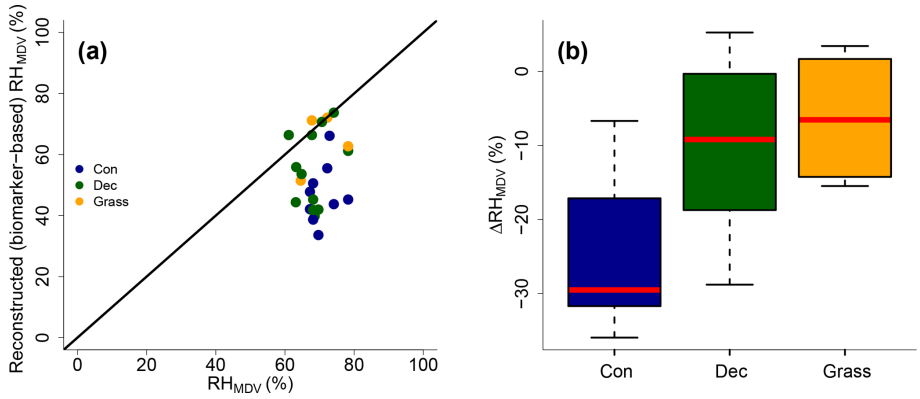

Figure 10. **(a)** Comparison of reconstructed (biomarker-based) RH_{MDV} values and climate station RH_{MDV} data. The black line indicates the 1 : 1 relationship. **(b)** Differences between reconstructed and climate station RH_{MDV} values (ΔRH_{MDV} = reconstructed − climate station RH_{MDV}) for the three different vegetation types along the transect. Abbreviations: con: coniferous forest sites ($n = 9$); dec: deciduous forest sites ($n = 11$); grass: grassland sites ($n = 4$).

and leaf water) along with vegetation types could also not be distinguished from signal damping effects.

The underestimation of RH for the deciduous and grass sites could be partly associated with the use of the GMWL as a baseline for the coupled $\delta^{2}H_{n\text{-alkane}}$–$\delta^{18}O_{sugar}$ approach. The deuterium excess of local meteoric water lines (LMWLs) is generally lower than the +10 ‰ of the GMWL, while the slopes of the LMWLs are comparable to the GMWL (Stumpp et al., 2014). In addition, if soil water evaporation occurred before water uptake by the plants, this would lead to an underestimation of biomarker-based RH_{MDV} values, too. It can be furthermore assumed that plant metabolism is highest during times with direct sunshine and high irradiation, i.e. during noon on sunny days. The relevant RH could therefore be lower than the climate-station-derived RH_{MDV}. Indeed, already climate station RH_{MDV} is considerably lower than RH_{MA} and RH_{MV} (Table S1 in the Supplement).

The uncertainty of reconstructed RH_{MDV} values is large for all three investigated vegetation types, and again these uncertainties are probably also related to ε_{bio}, which is most likely not constant as assumed for our calculations. Moreover, microclimate variability is underestimated in our approach. As mentioned in Sects. 2.4.2 and 3.7, in the coupled approach not only the source water of the plants is equated with (weighted) mean annual precipitation, but also an isotopic equilibrium between the source water and the (local) atmospheric water vapour is assumed. However, in areas with distinct seasonality this might be not fully valid. To account for this lack of equilibrium between precipitation and local atmospheric water vapour, apparent ε values can be calculated with data from Jacob and Sonntag (1991). As shown by Hepp et al. (2019) those values can be used to achieve alternative RH reconstructions based on the coupled $\delta^{2}H_{n\text{-alkane}}$–$\delta^{18}O_{sugar}$ approach. Such calculated RH_{MDV} values are on average 1.5 % more negative than the original values. However, this difference in RH is far below the analytical uncertainties of the compound-specific biomarker isotope analysis.

Finally, the integration time of the investigated topsoils has to be discussed. Unfortunately, no ^{14}C dates are available for the soil samples. However, most likely the organic matter has been built up over a longer timescale than the available climate data, which are used for comparison. In combination with vegetation changes/management changes throughout that period, this could surely lead to a less tight relationship of the reconstructions compared to the climate station data. Root input of arabinose and xylose seems to be of minor relevance in our topsoil samples. Otherwise, the reconstructed $\delta^{18}O_{sugar}$ values would be too negative, resulting in RH_{MDV} overestimations, which are not observed.

4 Conclusions

We were able to show the following.

i. The vegetation type does not significantly influence the brGDGT concentrations and proxies, yet the coniferous sites tend to have higher brGDGT concentrations, BIT indices and CBT-MBT′ ratios, while grass sites tend to be lowest.

ii. CBT faithfully records soil pH with a median ΔpH of 0.6 ± 0.6. The CBT overestimates the real pH in particular at the forest sites.

iii. CBT–MBT′-derived T_{MA} values reflect the climate-station-derived T_{MA} values with a median ΔT_{MA} of $0.5\,^{\circ}C \pm 2.4$, but again slightly too high reconstructions for the forest sites were observed.

iv. Differences in the apparent fractionation between the investigated vegetation types can be explained with signal damping.

v. The reconstructed $\delta^2H_{source\text{-}water}$ and $\delta^{18}O_{source\text{-}water}$ reflect the $\delta^2H_{GIPR,OIPC}$ and $\delta^{18}O_{GIPR,OIPC}$ with a systematic offset for δ^2H of $\sim -21‰ \pm 22‰$ and for $\delta^{18}O$ of $\sim -2.9‰ \pm 2.8‰$ (based on overall medians of $\Delta\delta^2H$, $\Delta\delta^{18}O$). This is caused by too negative reconstructions for coniferous and grass sites. For coniferous sites, this can be explained with *n*-alkanes originating from understorey grasses. As for the grass sites, the signal damping or variable ε_{bio} along with vegetation types affect δ^2H more than $\delta^{18}O$. This leads to too negative reconstructed $\delta^2H_{leaf\text{-}water}$ values and thus to too negative $\delta^2H_{source\text{-}water}$ and $\delta^{18}O_{source\text{-}water}$ reconstructions.

vi. Reconstructed (biomarker-based) RH_{MDV} values tend to underestimate climate-station-derived RH_{MDV} values ($\Delta RH_{MDV} = \sim -17\,\% \pm 12\,\%$). For coniferous sites the underestimations are strongest, which can be explained with understorey grasses being the main source of *n*-alkanes for the investigated soils under coniferous forests.

Overall, our study highlights the great potential of brGDGTs and the coupled $\delta^2H_{n\text{-}alkane}$–$\delta^{18}O_{sugar}$ approach for more quantitative paleoclimate reconstructions. Taking into account effects of different vegetation types improves correlations and reconstructions. This holds particularly true for the coupled $\delta^2H_{n\text{-}alkane}$–$\delta^{18}O_{sugar}$ approach, which is affected by signal damping of the grass vegetation or variable ε_{bio} (regarding ^2H between *n*-alkanes and leaf water) along with vegetation types. By contrast, vegetation-related effects do not strongly influence the brGDGT-derived reconstructions. Assuming constant ε_{bio} is likely a considerable source of uncertainty and should be further addressed in future field and/or modelling studies. Climate chamber experiments are most promising to further evaluate and refine the coupled $\delta^2H_{n\text{-}alkane}$–$\delta^{18}O_{sugar}$ approach, because uncertainties related to microclimate variability can be reduced. Field experiments like ours suffer from the fact that biomarker pools in the sampled topsoils may have been affected by past vegetation and climate changes and by the rather small range covered by the sampled transect. Both make the comparison between reconstructions and observations more difficult compared to large datasets and well-defined conditions.

Data availability. All the data used in this work are available via the Supplement.

Supplement. The supplement related to this article is available online at: https://doi.org/10.5194/bg-17-741-2020-supplement.

Author contributions. JH and IKS wrote the paper. MZ, RZ and JH acquired financial support. VL was responsible for field sampling and lipid analysis, and JH was responsible for sugar and pH analysis. IKS and JH acquired metadata and did the data evaluation. JF carried out the statistical analysis. VL, MB, KR, BG, MZ, TIE and RZ contributed to the discussion of the data and commented on the paper.

Competing interests. The authors declare that they have no conflict of interest.

Acknowledgements. We thank Lorenz Wüthrich, Heinz Veit, Tobias Sprafke, Alexander Groos (all University of Bern) and Anna-Saskia Kühnel (Technical University of Munich) for constructive discussions and statistical advice and Maria Schaarschmidt (University of Bayreuth), Corinna Heinrich and Marianne Benesch (Martin Luther University Halle-Wittenberg) for laboratory assistance during $\delta^{18}O_{sugar}$ analysis and pH measurements, respectively. Johannes Hepp greatly appreciates the support by the German Federal Environmental Foundation (DBU) in form of his PhD fellowship. This publication was funded by the German Research Foundation (DFG) and the University of Bayreuth in the funding programme Open Access Publishing.

Financial support. This research has been supported by the Swiss National Science Foundation (grant no. PP00P2 150590) and the German Federal Environmental Foundation (grant no. 20015/408).

This open-access publication was funded by the University of Bayreuth.

Review statement. This paper was edited by Marcel van der Meer and reviewed by two anonymous referees.

References

Allison, G. B., Gat, J. R., and Leaney, F. W. J.: The relationship between deuterium and oxygen-18 delta values in leaf water, Chem. Geol., 58, 145–156, 1985.

Amelung, W., Cheshire, M. V., and Guggenberger, G.: Determination of neutral and acidic sugars in soil by capillary gas-liquid chromatography after trifluoroacetic acid hydrolysis, Soil Biol. Biochem., 28, 1631–1639, 1996.

Anderson, V. J., Shanahan, T. M., Saylor, J. E., Horton, B. K., and Mora, A. R.: Sources of local and regional variability in the MBT′/CBT paleotemperature proxy: Insights from a modern elevation transect across the Eastern Cordillera of Colombia, Org. Geochem., 69, 42–51, https://doi.org/10.1016/j.orggeochem.2014.01.022, 2014.

Awe, G. O., Reichert, J. M., and Wendroth, O. O.: Temporal variability and covariance structures of soil temperature in a sugarcane field under different management practices in southern Brazil, Soil Till. Res., 150, 93–106, https://doi.org/10.1016/j.still.2015.01.013, 2015.

Bariac, T., Gonzalez-Dunia, J., Katerji, N., Béthenod, O., Bertolini, J. M., and Mariotti, A.: Spatial variation of the isotopic compo-

sition of water (^{18}O, ^{2}H) in the soil-plant-atmosphere system, 2. Assessment under field conditions, Chem. Geol., 115, 317–333, 1994.

Bowen, G. J.: The Online Isotopes in Precipitation Calculator, version 3.1., 2018.

Bowen, G. J. and Revenaugh, J.: Interpolating the isotopic composition of modern meteoric precipitation, Water Resour. Res., 39, 1–13, https://doi.org/10.1029/2003WR002086, 2003.

Brincat, D., Yamada, K., Ishiwatari, R., Uemura, H., and Naraoka, H.: Molecular-isotopic stratigraphy of long-chain *n*-alkanes in Lake Baikal Holocene and glacial age sediments, Org. Geochem., 31, 287–294, https://doi.org/10.1016/S0146-6380(99)00164-3, 2000.

Cappelen, J.: Danish Climatological Normals 1971–2000 – for selected stations, Danish Meteorological Institute, Copenhagen, 2002.

Cernusak, L. A., Wong, S. C., and Farquhar, G. D.: Oxygen isotope composition of phloem sap in relation to leaf water in Ricinus communis, Funct. Plant Biol., 30, 1059–1070, 2003.

Cernusak, L. A., Barbour, M. M., Arndt, S. K., Cheesman, A. W., English, N. B., Feild, T. S., Helliker, B. R., Holloway-Phillips, M. M., Holtum, J. A. M., Kahmen, A., Mcinerney, F. A., Munksgaard, N. C., Simonin, K. A., Song, X., Stuart-Williams, H., West, J. B., and Farquhar, G. D.: Stable isotopes in leaf water of terrestrial plants, Plant Cell Environ., 39, 1087–1102, https://doi.org/10.1111/pce.12703, 2016.

Christoph, H., Eglinton, T. I., Zech, W., Sosin, P., and Zech, R.: A 250 ka leaf-wax δD record from a loess section in Darai Kalon, Southern Tajikistan, Quaternary Sci. Rev., 208, 118–128, https://doi.org/10.1016/j.quascirev.2019.01.019, 2019.

Coffinet, S., Huguet, A., Anquetil, C., Derenne, S., Pedentchouk, N., Bergonzini, L., Omuombo, C., Williamson, D., Jones, M., Majule, A., and Wagner, T.: Evaluation of branched GDGTs and leaf wax *n*-alkane $\delta^{2}H$ as (paleo) environmental proxies in East Africa, Geochim. Cosmochim. Ac., 198, 182–193, https://doi.org/10.1016/j.gca.2016.11.020, 2017.

Cormier, M.-A., Werner, R. A., Sauer, P. E., Gröcke, D. R., M.C., L., Wieloch, T., Schleucher, J., and Kahmen, A.: ^{2}H fractiontions during the biosynthesis of carbohydrates and lipids imprint a metabolic signal on the $\delta^{2}H$ values of plant organic compounds, New Phytol., 218, 479–491, https://doi.org/10.1111/nph.15016, 2018.

Craig, H.: Isotopic Variations in Meteoric Waters, Science, 133, 1702–1703, 1961.

Dang, X., Yang, H., Naafs, B. D. A., Pancost, R. D., and Xie, S.: Evidence of moisture control on the methylation of branched glycerol dialkyl glycerol tetraethers in semi-arid and arid soils, Geochim. Cosmochim. Ac., 189, 24–36, https://doi.org/10.1016/j.gca.2016.06.004, 2016.

Dansgaard, W.: Stable isotopes in precipitation, Tellus, 16, 436–468, https://doi.org/10.1111/j.2153-3490.1964.tb00181.x, 1964.

Dawson, T. E., Mambelli, S., Plamboeck, A. H., Templer, P. H., and Tu, K. P.: Stable Isotopes in Plant Ecology, Annu. Rev. Ecol. Syst., 33, 507–559, https://doi.org/10.1146/annurev.ecolsys.33.020602.095451, 2002.

Diefendorf, A. F. and Freimuth, E. J.: Extracting the most from terrestrial plant-derived *n*-alkyl lipids and their carbon isotopes from the sedimentary record: A review, Org. Geochem., 103, 1–21, https://doi.org/10.1016/j.orggeochem.2016.10.016, 2016.

Dirghangi, S. S., Pagani, M., Hren, M. T., and Tipple, B. J.: Distribution of glycerol dialkyl glycerol tetraethers in soils from two environmental transects in the USA, Org. Geochem., 59, 49–60, https://doi.org/10.1016/j.orggeochem.2013.03.009, 2013.

Dubbert, M., Cuntz, M., Piayda, A., Maguás, C., and Werner, C.: Partitioning evapotranspiration – Testing the Craig and Gordon model with field measurements of oxygen isotope ratios of evaporative fluxes, J. Hydrol., 496, 142–153, https://doi.org/10.1016/j.jhydrol.2013.05.033, 2013.

DWD Climate Data Center: Historical annual precipitation observations for Germany, available at: https://opendata.dwd.de/climate_environment/CDC/observations_germany/climate/annual/more_precip/historical/, last access: 20 September 2018a.

DWD Climate Data Center: Historical hourly station observations of 2 m air temperature and humidity for Germany, available at: https://opendata.dwd.de/climate_environment/CDC/observations_germany/climate/hourly/air_temperature/historical/, last access: 19 September 2018b.

Eglinton, T. I. and Eglinton, G.: Molecular proxies for paleoclimatology, Earth Planet. Sc. Lett., 275, 1–16, 2008.

Feakins, S. J. and Sessions, A. L.: Controls on the D/H ratios of plant leaf waxes in an arid ecosystem, Geochim. Cosmochim. Ac., 74, 2128–2141, https://doi.org/10.1016/j.gca.2010.01.016, 2010.

Feakins, S. J., Bentley, L. P., Salinas, N., Shenkin, A., Blonder, B., Goldsmith, G. R., Ponton, C., Arvin, L. J., Wu, M. S., Peters, T., West, A. J., Martin, R. E., Enquist, B. J., Asner, G. P., and Malhi, Y.: Plant leaf wax biomarkers capture gradients in hydrogen isotopes of precipitation from the Andes and Amazon, Geochim. Cosmochim. Ac., 182, 155–172, https://doi.org/10.1016/j.gca.2016.03.018, 2016.

Freimuth, E. J., Diefendorf, A. F., and Lowell, T. V.: Hydrogen isotopes of *n*-alkanes and *n*-alkanoic acids as tracers of precipitation in a temperate forest and implications for paleorecords, Geochim. Cosmochim. Ac., 206, 166–183, https://doi.org/10.1016/j.gca.2017.02.027, 2017.

Frich, P., Rosenørn, S., Madsen, H., and Jensen, J. J.: Observed Precipitation in Denmark, 1961–90, Danish Meteorological Institute, Copenhagen, 1997.

Gamarra, B., Sachse, D., and Kahmen, A.: Effects of leaf water evaporative ^{2}H-enrichment and biosynthetic fractionation on leaf wax *n*-alkane $\delta^{2}H$ values in C_3 and C_4 grasses, Plant Cell Environ., 39, 2390–2403, https://doi.org/10.1111/pce.12789, 2016.

Gao, L., Edwards, E. J., Zeng, Y., and Huang, Y.: Major evolutionary trends in hydrogen isotope fractionation of vascular plant leaf waxes, PLoS ONE, 9, e112610, https://doi.org/10.1371/journal.pone.0112610, 2014.

Gat, J. R.: Comments on the Stable Isotope Method in Regional Groundwater Investigations, Water Resour. Res., 7, 980–993, https://doi.org/10.1029/WR007i004p00980, 1971.

Guggenberger, G., Christensen, B. T., and Zech, W.: Land-use effects on the composition of organic matter in particle-size separates of soil: I. Lignin and carbohydrate signature, Eur. J. Soil Sci., 45, 449–458, 1994.

Helliker, B. R. and Ehleringer, J. R.: Grass blades as tree rings: environmentally induced changes in the oxygen isotope ratio of cellu-

lose along the length of grass blades, New Phytol., 155, 417–424, 2002.

Hepp, J., Rabus, M., Anhäuser, T., Bromm, T., Laforsch, C., Sirocko, F., Glaser, B., and Zech, M.: A sugar biomarker proxy for assessing terrestrial versus aquatic sedimentary input, Org. Geochem., 98, 98–104, https://doi.org/10.1016/j.orggeochem.2016.05.012, 2016.

Hepp, J., Wüthrich, L., Bromm, T., Bliedtner, M., Schäfer, I. K., Glaser, B., Rozanski, K., Sirocko, F., Zech, R., and Zech, M.: How dry was the Younger Dryas? Evidence from a coupled δ^2H–δ^{18}O biomarker paleohygrometer applied to the Gemündener Maar sediments, Western Eifel, Germany, Clim. Past, 15, 713–733, https://doi.org/10.5194/cp-15-713-2019, 2019.

Herrmann, A., Maloszewski, P., and Stichler, W.: Changes of ^{18}O contents of precipitation water during seepage in the unsaturated zone, in: Proceedings of International Symposium on Groundwater Monitoring and Management, 23–28 March 1987, p. 22, Institut of Water Management Berlin (GDR) with support of UNESCO, Dresden, 1987.

Hopmans, E. C., Weijers, J. W. H., Schefuß, E., Herfort, L., Sinninghe Damsté, J. S., and Schouten, S.: A novel proxy for terrestrial organic matter in sediments based on branched and isoprenoid tetraether lipids, Earth Planet. Sc. Lett., 224, 107–116, https://doi.org/10.1016/j.epsl.2004.05.012, 2004.

Horita, J. and Wesolowski, D. J.: Liquid-vapor fractionation of oxygen and hydrogen isotopes of water from the freezing to the critical temperature, Geochim. Cosmochim. Ac., 58, 3425–3437, https://doi.org/10.1016/0016-7037(94)90096-5, 1994.

Hothorn, T., Bühlmann, P., Dudoit, S., Molinaro, A., and Van Der Laan, M. J.: Survival ensembles, Biostatistics, 7, 355–373, https://doi.org/10.1093/biostatistics/kxj011, 2006.

Hou, J., D'Andrea, W. J., and Huang, Y.: Can sedimentary leaf waxes record D/H ratios of continental precipitation? Field, model, and experimental assessments, Geochim. Cosmochim. Ac., 72, 3503–3517, https://doi.org/10.1016/j.gca.2008.04.030, 2008.

Huguet, A., Fosse, C., Metzger, P., Fritsch, E., and Derenne, S.: Occurrence and distribution of extractable glycerol dialkyl glycerol tetraethers in podzols, Org. Geochem., 41, 291–301, https://doi.org/10.1016/j.orggeochem.2009.10.007, 2010a.

Huguet, A., Fosse, C., Laggoun-Défarge, F., Toussaint, M. L., and Derenne, S.: Occurrence and distribution of glycerol dialkyl glycerol tetraethers in a French peat bog, Org. Geochem., 41, 559–572, https://doi.org/10.1016/j.orggeochem.2010.02.015, 2010b.

IAEA/WMO: Global Network of Isotopes in Precipitation, The GNIP Database, available at: https://nucleus.iaea.org/wiser, 2015.

IAEA/WMO: Global Network of Isotopes in Precipitation, The GNIP Database, available at: https://nucleus.iaea.org/wiser, last access: 18 September 2018.

Jacob, H. and Sonntag, C.: An 8-year record of the seasonal-variation of ^{2}H and ^{18}O in atmospheric water vapor and precipitation at Heidelberg, Tellus B, 43, 291–300, 1991.

De Jonge, C., Hopmans, E. C., Zell, C. I., Kim, J. H., Schouten, S., and Sinninghe Damsté, J. S.: Occurrence and abundance of 6-methyl branched glycerol dialkyl glycerol tetraethers in soils: Implications for palaeoclimate reconstruction, Geochim. Cosmochim. Ac., 141, 97–112, https://doi.org/10.1016/j.gca.2016.03.038, 2014.

Kahmen, A., Schefuß, E., and Sachse, D.: Leaf water deuterium enrichment shapes leaf wax n-alkane δD values of angiosperm plants I: Experimental evidence and mechanistic insights, Geochim. Cosmochim. Ac., 111, 39–49, https://doi.org/10.1016/j.gca.2012.09.004, 2013.

Knapp, D. R.: Handbook of Analytical Derivatization Reactions, John Wiley & Sons, New York, Chichester, Brisbane, Toronto, Singapore, 1979.

Konecky, B., Dee, S. G., and Noone, D. C.: WaxPSM: A Forward Model of Leaf Wax Hydrogen Isotope Ratios to Bridge Proxy and Model Estimates of Past Climate, J. Geophys. Res.-Biogeo., 124, 2107–2125, https://doi.org/10.1029/2018JG004708, 2019.

Laursen, E. V., Thomsen, R. S., and Cappelen, J.: Observed Air Temperature, Humidity, Pressure, Cloud Cover and Weather in Denmark – with Climatological Standard Normals, 1961–90, Danish Meteorological Institute, Copenhagen, 1999.

Levene, H.: Robust Tests for Equality of Variances, in: Contributions to Probability and Statistics: Essays in Honor of Harold Hotelling, Vol. 69, edited by: Olkin, I., 78–92, Standford University Press, Palo Alto, California, 1960.

Liu, H. T., Schäufele, R., Gong, X. Y., and Schnyder, H.: The δ^{18}O and δ^2H of water in the leaf growth-and-differentiation zone of grasses is close to source water in both humid and dry atmospheres, New Phytol., 214, 1423–1431, https://doi.org/10.1111/nph.14549, 2017.

Liu, J., Liu, W., An, Z., and Yang, H.: Different hydrogen isotope fractionations during lipid formation in higher plants: Implications for paleohydrology reconstruction at a global scale, Sci. Rep.-UK, 6, 19711, https://doi.org/10.1038/srep19711, 2016.

Liu, W. and Yang, H.: Multiple controls for the variability of hydrogen isotopic compositions in higher plant n-alkanes from modern ecosystems, Glob. Change Biol., 14, 2166–2177, https://doi.org/10.1111/j.1365-2486.2008.01608.x, 2008.

Liu, Y., Wang, J., Liu, D., Li, Z., Zhang, G., Tao, Y., Xie, J., Pan, J., and Chen, F.: Straw mulching reduces the harmful effects of extreme hydrological and temperature conditions in citrus orchards, PLoS ONE, 9, 1–9, https://doi.org/10.1371/journal.pone.0087094, 2014.

McInerney, F. A., Helliker, B. R., and Freeman, K. H.: Hydrogen isotope ratios of leaf wax n-alkanes in grasses are insensitive to transpiration, Geochim. Cosmochim. Ac., 75, 541–554, https://doi.org/10.1016/j.gca.2010.10.022, 2011.

Merlivat, L.: Molecular diffusivities of $H_2^{16}O$, $HD^{16}O$, and $H_2^{18}O$ in gases, J. Chem. Phys., 69, 2864–2871, https://doi.org/10.1063/1.436884, 1978.

Mueller-Niggemann, C., Utami, S. R., Marxen, A., Mangelsdorf, K., Bauersachs, T., and Schwark, L.: Distribution of tetraether lipids in agricultural soils – differentiation between paddy and upland management, Biogeosciences, 13, 1647–1666, https://doi.org/10.5194/bg-13-1647-2016, 2016.

Oppermann, B. I., Michaelis, W., Blumenberg, M., Frerichs, J., Schulz, H. M., Schippers, A., Beaubien, S. E., and Krüger, M.: Soil microbial community changes as a result of long-term exposure to a natural CO_2 vent, Geochim. Cosmochim. Ac., 74, 2697–2716, https://doi.org/10.1016/j.gca.2010.02.006, 2010.

Pedentchouk, N. and Zhou, Y.: Factors Controlling Carbon and Hydrogen Isotope Fractionation During Biosynthesis of Lipids by

Phototrophic Organisms, in: Hydrocarbons, Oils and Lipids: Diversity, Origin, Chemistry and Fate. Handbook of Hydrocarbon and Lipid Microbiology, edited by: Wilkes, H., 1–24, Springer, Cham., 2018.

Peterse, F., van der Meer, J., Schouten, S., Weijers, J. W. H., Fierer, N., Jackson, R. B., Kim, J. H., and Sinninghe Damsté, J. S.: Revised calibration of the MBT-CBT paleotemperature proxy based on branched tetraether membrane lipids in surface soils, Geochim. Cosmochim. Ac., 96, 215–229, https://doi.org/10.1016/j.gca.2012.08.011, 2012.

Prietzel, J., Dechamps, N., and Spielvogel, S.: Analysis of noncellulosic polysaccharides helps to reveal the history of thick organic surface layers on calcareous Alpine soils, Plant Soil, 365, 93–114, https://doi.org/10.1007/s11104-012-1340-2, 2013.

Rach, O., Brauer, A., Wilkes, H., and Sachse, D.: Delayed hydrological response to Greenland cooling at the onset of the Younger Dryas in western Europe, Nat. Geosci., 7, 109–112, https://doi.org/10.1038/ngeo2053, 2014.

Rao, Z., Zhu, Z., Jia, G., Henderson, A. C. G., Xue, Q., and Wang, S.: Compound specific δD values of long chain *n*-alkanes derived from terrestrial higher plants are indicative of the δD of meteoric waters: Evidence from surface soils in eastern China, Org. Geochem., 40, 922–930, https://doi.org/10.1016/j.orggeochem.2009.04.011, 2009.

R Core Team: R: A Language and Environment for Statistical Computing, available at: https://www.r-project.org/, last access: 14 August 2015.

Romero-Viana, L., Kienel, U., and Sachse, D.: Lipid biomarker signatures in a hypersaline lake on Isabel Island (Eastern Pacific) as a proxy for past rainfall anomaly (1942–2006 AD), Palaeogeogr. Palaeocl., 350–352, 49–61, https://doi.org/10.1016/j.palaeo.2012.06.011, 2012.

Sachse, D., Radke, J., and Gleixner, G.: Hydrogen isotope ratios of recent lacustrine sedimentary *n*-alkanes record modern climate variability, Geochim. Cosmochim. Ac., 68, 4877–4889, https://doi.org/10.1016/j.gca.2004.06.004, 2004.

Sachse, D., Radke, J., and Gleixner, G.: δD values of individual *n*-alkanes from terrestrial plants along a climatic gradient – Implications for the sedimentary biomarker record, Org. Geochem., 37, 469–483, https://doi.org/10.1016/j.orggeochem.2005.12.003, 2006.

Sachse, D., Billault, I., Bowen, G. J., Chikaraishi, Y., Dawson, T. E., Feakins, S. J., Freeman, K. H., Magill, C. R., McInerney, F. A., van der Meer, M. T. J., Polissar, P., Robins, R. J., Sachs, J. P., Schmidt, H.-L., Sessions, A. L., White, J. W. C., and West, J. B.: Molecular Paleohydrology: Interpreting the Hydrogen-Isotopic Composition of Lipid Biomarkers from Photosynthesizing Organisms, Annu. Rev., 40, 221–249, https://doi.org/10.1146/annurev-earth-042711-105535, 2012.

Schäfer, I. K., Lanny, V., Franke, J., Eglinton, T. I., Zech, M., Vysloužilová, B., and Zech, R.: Leaf waxes in litter and topsoils along a European transect, SOIL, 2, 551–564, https://doi.org/10.5194/soil-2-551-2016, 2016.

Schlotter, D.: The spatio-temporal distribution of $\delta^{18}O$ and $\delta^{2}H$ of precipitation in Germany – an evaluation of regionalization methods, Albert-Ludwigs-Universität Freiburg im Breisgau, available at: http://www.hydrology.uni-freiburg.de/abschluss/Schlotter_D_2007_DA.pdf (last access: 9 September 2018), 2007.

Schmidt, H.-L., Werner, R. A., and Roßmann, A.: ^{18}O Pattern and biosynthesis of natural plant products, Phytochemistry, 58, 9–32, https://doi.org/10.1016/S0031-9422(01)00017-6, 2001.

Schmidt, H.-L., Werner, R. A., and Eisenreich, W.: Systematics of ^{2}H patterns in natural compounds and its importance for the elucidation of biosynthetic pathways, Phytochem. Rev., 2, 61–85, https://doi.org/10.1023/B:PHYT.0000004185.92648.ae, 2003.

Schouten, S., Hopmans, E. C., and Sinninghe Damsté, J. S.: The organic geochemistry of glycerol dialkyl glycerol tetraether lipids: A review, Org. Geochem., 54, 19–61, https://doi.org/10.1016/j.orggeochem.2012.09.006, 2013.

Schreuder, L. T., Beets, C. J., Prins, M. A., Hatté, C., and Peterse, F.: Late Pleistocene climate evolution in Southeastern Europe recorded by soil bacterial membrane lipids in Serbian loess, Palaeogeogr. Palaeocl., 449, 141–148, https://doi.org/10.1016/j.palaeo.2016.02.013, 2016.

Sessions, A. L., Burgoyne, T. W., Schimmelmann, A., and Hayes, J. M.: Fractionation of hydrogen isotopes in lipid biosynthesis, Org. Geochem., 30, 1193–1200, 1999.

Shapiro, S. S. and Wilk, M. B.: An Analysis of Variance Test for Normality, Biometrika, 52, 591–611, https://doi.org/10.2307/2333709, 1965.

Sternberg, L. S. L.: Comment on "Oxygen isotope ratios ($^{18}O/^{16}O$) of hemicellulose-derived sugar biomarkers in plants, soils and sediments as paleoclimate proxy I: Insight from a climate chamber experiment" by Zech et al. (2014), Geochim. Cosmochim. Ac., 141, 677–679, https://doi.org/10.1016/j.gca.2014.04.051, 2014.

Strobl, C., Boulesteix, A. L., Zeileis, A., and Hothorn, T.: Bias in random forest variable importance measures: Illustrations, sources and a solution, BMC Bioinformatics, 8, 25, https://doi.org/10.1186/1471-2105-8-25, 2007.

Strobl, C., Boulesteix, A. L., Kneib, T., Augustin, T., and Zeileis, A.: Conditional variable importance for random forests, BMC Bioinformatics, 9, 1–11, https://doi.org/10.1186/1471-2105-9-307, 2008.

Stumpp, C., Klaus, J., and Stichler, W.: Analysis of long-term stable isotopic composition in German precipitation, J. Hydrol., 517, 351–361, https://doi.org/10.1016/j.jhydrol.2014.05.034, 2014.

Sun, C. J., Zhang, C. L., Li, F. Y., Wang, H. Y., and Liu, W. G.: Distribution of branched glycerol dialkyl glycerol tetraethers in soils on the Northeastern Qinghai-Tibetan Plateau and possible production by nitrite-reducing bacteria, Sci. China Earth Sci., 59, 1834–1846, https://doi.org/10.1007/s11430-015-0230-2, 2016.

Swedish Meteorological and Hydrological Institute: SMHI Open Data Meteorological Observations, available at: https://opendata-download-metobs.smhi.se/explore/, last access: 19 September 2018.

Tipple, B. J., Berke, M. A., Hambach, B., Roden, J. S., and Ehleringer, J. R.: Predicting leaf wax *n*-alkane $^{2}H/^{1}H$ ratios: Controlled water source and humidity experiments with hydroponically grown trees confirm predictions of Craig-Gordon model, Plant Cell Environ., 38, 1035–1047, https://doi.org/10.1111/pce.12457, 2015.

Tuthorn, M., Zech, M., Ruppenthal, M., Oelmann, Y., Kahmen, A., del Valle, H. F., Wilcke, W., and Glaser, B.: Oxygen isotope ratios ($^{18}O/^{16}O$) of hemicellulose-derived sugar biomarkers in plants, soils and sediments as paleoclimate proxy II: Insight from a cli-

mate transect study, Geochim. Cosmochim. Ac., 126, 624–634, https://doi.org/10.1016/j.gca.2013.11.002, 2014.

Tuthorn, M., Zech, R., Ruppenthal, M., Oelmann, Y., Kahmen, A., del Valle, H. F., Eglinton, T., Rozanski, K., and Zech, M.: Coupling $\delta^{2}H$ and $\delta^{18}O$ biomarker results yields information on relative humidity and isotopic composition of precipitation – a climate transect validation study, Biogeosciences, 12, 3913–3924, https://doi.org/10.5194/bg-12-3913-2015, 2015.

Umweltbundesamt GmbH: Erhebung der Wassergüte in Österreich gemäß Hydrographiegesetz i.d.F. des BGBl. Nr. 252/90 (gültig bis Dezember 2006) bzw. Gewässerzustandsüberwachung in Österreich gemäß Wasserrechtsgesetz, BGBl. I Nr. 123/06, i.d.g.F.; BMLFUW, Sektion IV/Abteilung 3 N, available at: https://wasser.umweltbundesamt.at/h2odb/fivestep/abfrageQdPublic.xhtml, last access: 20 September 2018.

van Geldern, R., Baier, A., Subert, H. L., Kowol, S., Balk, L., and Barth, J. A. C.: (Table S1) Stable isotope composition of precipitation sampled at Erlangen, Germany between 2010 and 2013 for station GeoZentrum located at Erlangen city center, supplement to: van Geldern, R. et al. (2014): Pleistocene paleo-groundwater as a pristine fresh water resource in southern Germany – evidence from stable and radiogenic isotopes, Sci. Total Environ., PANGAEA, https://doi.org/10.1594/PANGAEA.833837, 2014.

Walker, C. D. and Brunel, J.-P.: Examining Evapotranspiration in a Semi-Arid Region using Stable Isotopes of Hydrogen and Oxygen, J. Hydrol., 118, 55–75, 1990.

Wang, C., Hren, M. T., Hoke, G. D., Liu-Zeng, J., and Garzione, C. N.: Soil n-alkane δD and glycerol dialkyl glycerol tetraether (GDGT) distributions along an altitudinal transect from southwest China: Evaluating organic molecular proxies for paleoclimate and paleoelevation, Org. Geochem., 107, 21–32, https://doi.org/10.1016/j.orggeochem.2017.01.006, 2017.

Wang, H., Liu, W., Zhang, C. L., Liu, Z., and He, Y.: Branched and isoprenoid tetraether (BIT) index traces water content along two marsh-soil transects surrounding Lake Qinghai: Implications for paleo-humidity variation, Org. Geochem., 59, 75–81, https://doi.org/10.1016/j.orggeochem.2013.03.011, 2013.

Weijers, J. W. H., Schouten, S., Spaargaren, O. C., and Sinninghe Damsté, J. S.: Occurrence and distribution of tetraether membrane lipids in soils: Implications for the use of the TEX_{86} proxy and the BIT index, Org. Geochem., 37, 1680–1693, https://doi.org/10.1016/j.orggeochem.2006.07.018, 2006.

Weijers, J. W. H., Schouten, S., van den Donker, J. C., Hopmans, E. C., and Sinninghe Damsté, J. S.: Environmental controls on bacterial tetraether membrane lipid distribution in soils, Geochim. Cosmochim. Ac., 71, 703–713, https://doi.org/10.1016/j.gca.2006.10.003, 2007.

Weijers, J. W. H., Wiesenberg, G. L. B., Bol, R., Hopmans, E. C., and Pancost, R. D.: Carbon isotopic composition of branched tetraether membrane lipids in soils suggest a rapid turnover and a heterotrophic life style of their source organism(s), Biogeosciences, 7, 2959–2973, https://doi.org/10.5194/bg-7-2959-2010, 2010.

Weijers, J. W. H., Steinmann, P., Hopmans, E. C., Schouten, S., and Sinninghe Damsté, J. S.: Bacterial tetraether membrane lipids in peat and coal: Testing the MBT-CBT temperature proxy for climate reconstruction, Org. Geochem., 42, 477–486, https://doi.org/10.1016/j.orggeochem.2011.03.013, 2011.

Xie, S., Pancost, R. D., Chen, L., Evershed, R. P., Yang, H., Zhang, K., Huang, J., and Xu, Y.: Microbial lipid records of highly alkaline deposits and enhanced aridity associated with significant uplift of the Tibetan Plateau in the Late Miocene, Geology, 40, 291–294, https://doi.org/10.1130/G32570.1, 2012.

Zech, M. and Glaser, B.: Compound-specific $\delta^{18}O$ analyses of neutral sugars in soils using gas chromatography-pyrolysis-isotope ratio mass spectrometry: problems, possible solutions and a first application, Rapid Commun. Mass Sp., 23, 3522–3532, https://doi.org/10.1002/rcm.4278, 2009.

Zech, M., Rass, S., Buggle, B., Löscher, M., and Zöller, L.: Reconstruction of the late Quaternary paleoenvironments of the Nussloch loess paleosol sequence, Germany, using n-alkane biomarkers, Quaternary Res., 78, 226–235, https://doi.org/10.1016/j.yqres.2012.05.006, 2012a.

Zech, M., Kreutzer, S., Goslar, T., Meszner, S., Krause, T., Faust, D., and Fuchs, M.: Technical Note: n-Alkane lipid biomarkers in loess: post-sedimentary or syn-sedimentary?, Biogeosciences Discuss., 9, 9875–9896, https://doi.org/10.5194/bgd-9-9875-2012, 2012b.

Zech, M., Tuthorn, M., Detsch, F., Rozanski, K., Zech, R., Zöller, L., Zech, W., and Glaser, B.: A 220 ka terrestrial $\delta^{18}O$ and deuterium excess biomarker record from an eolian permafrost paleosol sequence, NE-Siberia, Chem. Geol., 360–361, 220–230, https://doi.org/10.1016/j.chemgeo.2013.10.023, 2013.

Zech, M., Mayr, C., Tuthorn, M., Leiber-Sauheitl, K., and Glaser, B.: Reply to the comment of Sternberg on "Zech et al. (2014) Oxygen isotope ratios ($^{18}O/^{16}O$) of hemicellulose-derived sugar biomarkers in plants, soils and sediments as paleoclimate proxy I: Insight from a climate chamber experiment. GCA, Geochim. Cosmochim. Ac., 141, 680–682, https://doi.org/10.1016/j.gca.2014.04.051, 2014.

Zech, M., Zech, R., Rozanski, K., Gleixner, G., and Zech, W.: Do n-alkane biomarkers in soils/sediments reflect the $\delta^{2}H$ isotopic composition of precipitation? A case study from Mt. Kilimanjaro and implications for paleoaltimetry and paleoclimate research, Isot. Environ. Healt. S., 51, 508–524, https://doi.org/10.1080/10256016.2015.1058790, 2015.

Zech, R., Gao, L., Tarozo, R., and Huang, Y.: Branched glycerol dialkyl glycerol tetraethers in Pleistocene loess-paleosol sequences: Three case studies, Org. Geochem., 53, 38–44, https://doi.org/10.1016/j.orggeochem.2012.09.005, 2012.